

Perturbation Approach to the Self Energy of non-S Hydrogenic States

Eric-Olivier Le Bigot,^{1,2} Ulrich D. Jentschura,^{1,3} Peter J. Mohr,² Paul Indelicato,¹ and Gerhard So³

¹Laboratoire Kastler Brossel, Ecole Normale Supérieure et Université Pierre et Marie Curie, Case 74, 75005 Paris, France

²National Institute of Standards and Technology, Mail Stop 8401, Gaithersburg, MD 20899-8401, USA

³Institut für Theoretische Physik, Technische Universität Dresden, 01062 Dresden, Germany

We present results on the self-energy correction to the energy levels of hydrogen and hydrogenlike ions. The self energy represents the largest QED correction to relativistic (Dirac-Coulomb) energy levels. We focus on the perturbation expansion of the self energy of non-S states, and provide estimates of the Bethe logarithm and of the so-called A_{60} perturbative coefficient, which can be considered as a relativistic Bethe logarithm. All non-S atomic states are covered. These results can be used in high-precision spectroscopy experiments in hydrogen and hydrogenlike ions. They yield the best available estimate of the self-energy correction of many atomic states.

PACS numbers: 12.20.Ds, 31.30.Jv, 06.20.Jr, 31.15.-p

I. INTRODUCTION

The recent dramatic progress¹ in high-precision spectroscopy (see, e.g., [1]) has motivated the calculation of numerous contributions to the energy levels of hydrogen and hydrogenlike systems. Such spectroscopic experiments test our understanding of atomic levels, and provide precise determinations of fundamental constants [2]; this requires accurate predictions of atomic energies, and, in particular, the calculation of corrections due to Quantum Electrodynamics (QED), the quantum field theory of electromagnetic interactions. In hydrogen and hydrogenlike ions, the largest correction to the relativistic (Dirac) energy levels is provided by the so-called self-energy contribution of QED. The self energy is a process which modifies the relativistic (Dirac) energy of an electron, and which can be depicted by the following Feynman diagram,



where the double line denotes the electron (bound to the nucleus), and where the wavy line represents the photon emitted and reabsorbed by the electron. The self-energy correction to energy levels in hydrogen and hydrogenlike ions can be expressed as an expansion in Z and $\ln(Z)$ (see, e.g., [3]) | Z is the nuclear charge number of the nucleus of the hydrogenlike ion under consideration, and α is the fine-structure constant. Analytic calculations of the (one-loop) self energy in bound systems have a long history, starting from Bethe's seminal paper [4], and have since extended over more than five decades.

The purpose of this paper is to provide good approximate values of the self-energy correction to the energy levels of hydrogen and hydrogenlike ions, for any P state, and any state with a higher angular momentum. Only a part of the perturbation expansion of the self energy of these states is known analytically. The first two non-analytically-known contributions to this expansion are the Bethe logarithm $\ln k_0(nl)$ and the so-called $A_{60}(nl_j)$ coefficient of the self energy, which can be characterized

as a relativistic Bethe logarithm [see Sec. II, and in particular Eqs. (1), (7) and (8)]. Here, nl_j is the standard spectroscopic notation for an atomic state. This paper thus contains formulas for estimating both of these important quantities (see Sec. V and VI).

Very precise numerical values of the Bethe logarithm $\ln k_0(nl)$ have been obtained (see, e.g., Ref. [5]), and numerical convergence acceleration techniques [6] can in principle yield very precise values of this quantity for any atomic state nl [see also Eq. (34) below]. The estimate that we provide in Sec. VI should be useful to experiments that use levels for which no published values exist (see, e.g., Ref. [7]).

Many new values of the relativistic Bethe logarithm $A_{60}(nl_j)$ have recently been published [8]. Other values have been obtained previously for some S [9, 10, 11] and P states [12, 13]. This paper contains two additional values [$A_{60}(5F_{5=2})$ and $A_{60}(5F_{7=2})$], as well as details on the procedure that we used in obtaining the values of A_{60} in Ref. [8] and in Table III (see Sec. IV).

The results of Sec. IV (VI) provide an improvement over the available approximations of the bound-electron self energy, over a large range of nuclear charge numbers Z . In particular, they yield the best available estimates for the self-energy correction in hydrogen, for all the states for which no exact (non-perturbative) value of the self energy has yet been published (i.e., all levels, except $n=1$ and $n=2$ levels [1, 14]).

It is important to know accurately the energy (and in particular the self energy) of higher angular momentum states, because they are used in high-precision spectroscopic measurements [15, 16, 17, 18, 19, 20]. States with very-high angular orbital quantum numbers $l' \geq 30$ have been recently used in such experiments [7]. Further motivation for the present study results from the need to accurately compare the two approaches that have been used for the theoretical study of QED shifts, so as to check their consistency: (i) the analytic expansion in the parameter Z^{-1} , mostly used for low- Z systems, and (ii) the numerical approach, which avoids the Z^{-1} expansion and has been used predominantly for the theoretical description of high- Z hydrogenlike ions [21].

Recently, the most accurate methods in implementing a non-perturbative calculation of the self energy [14, 22, 23, 24, 25] have been extended by analytic results [26] that, taken together, provide access to the self-energy shift of electrons of total angular momentum $j > 3/2$. This has allowed us to obtain numerical values of the self energy, and to use them in checks of the A_{60} coefficients presented in Tables I{IV (see Sec. V II).

Moreover, general progress in theoretical calculations of atomic energy levels has been achieved by means of numerical algorithms [6, 25, 27] that lead to an accelerated convergence of the angular momentum series expansion of the bound-electron relativistic Green function. Such algorithms are also useful for performing the series summations that we had to do in order to obtain the values of A_{60} presented here (see Sec. IV).

Notation and conventions are defined in Sec. II. The mathematical method used for the semi-analytic calculations of A_{60} in Ref. [8] is discussed in Sec. III. Details on these calculations are presented in Sec. IV. Formulas for the relativistic Bethe logarithm $A_{60}(n_l_j)$ of S and P states are presented in Sec. V. Estimates of the Bethe logarithm $\ln k_0(n_l)$ and of $A_{60}(n_l_j)$ as a function of the orbital quantum number l are reported in Sec. VI. We have performed additional checks of the values of A_{60} in Tables I{IV, as described in Sec. V II; we also show in that section that the inclusion of A_{60} in the (truncated) perturbation expansion of the electron self energy does indeed improve the self energy estimates. A summary of the paper is given in Sec. V III. The fitting method that we used in obtaining asymptotic behaviors of $\ln k_0(n_l)$ and of $A_{60}(n_l_j)$ is described in the Appendix.

II. NOTATION AND CONVENTIONS

In this section, we define the notation and conventions used in this paper. We write the (real part of the) one-loop self-energy shift of an electron in the level n with orbital angular momentum l and total angular momentum j as

$$E_{SE} = -\frac{(Z)^4}{n^3} F(n_l_j; Z) m c^2; \quad (1)$$

where $F(n_l_j; Z)$ is a dimensionless quantity. We use natural units, in which $\hbar = c = m = 1$ and $e^2 = 4$ (m is the electron mass). It is customary in the literature to suppress the dependence of F on the quantum numbers n , j and l and write $F(Z)$ for $F(n_l_j; Z)$.

The quantum numbers l and j can be combined into the Dirac angular quantum number κ . As a function of j and l , κ is given by

$$\kappa = 2(l - j)(j + 1/2); \quad (2a)$$

ie.,

$$\kappa = (j + 1/2) \text{ for } j = l + 1/2; \quad (2b)$$

and

$$\kappa = (j + 1/2) \text{ for } j = l - 1/2; \quad (2c)$$

The quantum numbers j and l can be derived from according to

$$l = j + 1/2 \text{ for } j = 1/2, 3/2, \dots \quad (3)$$

and

$$l = j \text{ for } j = 1/2, 3/2, \dots \quad (4)$$

ie., specifies uniquely both j and l . The semi-analytic expansion of $F(n_l_j; Z)$ about $Z = 0$ for a general atomic state with quantum numbers n , l and j gives rise to the expression [3]

$$\begin{aligned} F(n_l_j; Z) = & A_{41}(n_l_j) \ln[(Z)^2] \\ & + A_{40}(n_l_j) + (Z) A_{50}(n_l_j) \\ & + (Z)^2 A_{62}(n_l_j) \ln^2[(Z)^2] \\ & + A_{61}(n_l_j) \ln[(Z)^2] \\ & + G_{SE}(n_l_j; Z) : \end{aligned} \quad (5)$$

This expansion is semi-analytic, ie., it involves powers of Z and of $\ln[(Z)^2]$. Terms added to the leading order in Z are commonly referred to as the binding corrections. The A coefficients have two indices, the first of which denotes the power of Z [including those powers contained in Eq. (1)], while the second index denotes the power of the logarithm $\ln[(Z)^2]$.

The limit as $Z \rightarrow 0$ of $G_{SE}(n_l_j; Z)$ is known to be finite and is referred to as the A_{60} coefficient, ie.,

$$A_{60}(n_l_j) = \lim_{Z \rightarrow 0} G_{SE}(n_l_j; Z); \quad (6)$$

Historically, the evaluation of the coefficient A_{60} has been highly problematic. Due to the large number of terms that contribute at relative order $(Z)^2$ and problems concerning the separation of terms that contribute at a specific order in the Z expansion, evaluations are plagued with severe calculational as well as conceptual difficulties. For example, the evaluation of $A_{60}(1S_{1=2})$ has drawn a lot of attention for a long time [3, 10, 28, 29, 30]. And in general, the complexity of the calculation increases with increasing principal quantum number.

For particular states, some of the coefficients in (5) vanish. Notably, this is the case for P states and for states with higher angular momenta, as a consequence of their behavior at the origin, which is less singular than that of S states (specifically, we have $A_{62}(n_l_j) = A_{50}(n_l_j) = A_{41}(n_l_j) = 0$ for $l \neq 0$ | see Refs. [3, 28] and references therein). The fact that the logarithmic coefficient $A_{71}(n_l_j)$ vanishes for $l \neq 0$ has been pointed out in [31]. For nonzero l , we thus have

$$\begin{aligned} F(n_l_j; Z) = & A_{40}(n_l_j) + (Z)^2 A_{61}(n_l_j) \ln[(Z)^2] \\ & + A_{60}(n_l_j) + O[(Z)^3] \quad (l \neq 0); \end{aligned} \quad (7)$$

For the comparison to experimental data, it is useful to note that the terms in (5) and (7) acquire reduced-mass corrections according to Eqs. (2.5a) and (2.5b) of [32].

The general formula for A_{40} for a non-S state reads (see, e.g., [2, 3, 32])

$$A_{40} = \frac{1}{2} \frac{1}{(2l+1)} \frac{4}{3} \ln k_0(nl); \quad (8)$$

where the Bethe logarithm $\ln k_0(nl)$ is an inherently non-relativistic quantity, whose expression reads

$$\ln k_0(nl) = \frac{n^3}{2(Z)^4 m} \frac{p^i}{m} (H_S - E_n) \ln 2 \frac{H_S - E_n}{(Z)^2 m} \frac{p^i}{m} : \quad (9)$$

The ket $|j\rangle$ represents the Schrodinger wave function, the p^i are the components of the momentum operator, the Hamiltonian H_S is the nonrelativistic operator $p^2 = (2m)^{-1} (Z)^{-2} = r^{-2}$, and E_n is the Schrodinger bound-state energy $(Z)^{-2} m = (2n^2)^{-1}$. The Bethe logarithm is spin-independent and therefore independent of the total angular momentum j for a given orbital angular momentum l ; it can be written as a function of n and l alone. For the atomic levels under investigation, the Bethe logarithm has been evaluated in [33] and [5, 34, 35, 36, 37, 38, 39, 40] (the results exhibit varying accuracies). Because A_{60} involves relativistic corrections to the coefficient A_{40} , which in turn is given mainly by the Bethe logarithm, it is natural to refer to A_{60} as a "relativistic Bethe logarithm."

A general analytic result for the logarithmic correction A_{61} as a function of the bound state quantum numbers n, l and j can be inferred from Eq. (4.4a) of [3, 28] upon subtraction of the vacuum polarization contribution contained in the quoted equation. We have ($\dot{}$ denotes the logarithmic derivative of the function [41, x 6.3])

$$A_{61}(nl_j) = \frac{4}{3} \frac{(8(1-l) + 3) \frac{1(l+1)}{n^2}}{\sum_{m=1}^{\infty} (2l+m)} \quad (10)$$

$$+ \frac{1}{n^2} \left(\frac{1}{10} + \frac{1}{4} \right) \frac{1}{j+1} + \frac{601}{240} \frac{77}{60n^2}$$

$$+ 7 \ln 2 + 3 \left(\ln n + \ln(n+1) \right) :$$

We may infer immediately

$$A_{61}(nP_{1=2}) = \frac{1}{45} \left(33 - \frac{29}{n^2} \right); \quad (11a)$$

$$A_{61}(nP_{3=2}) = \frac{2}{45} \left(9 - \frac{7}{n^2} \right); \quad (11b)$$

$$A_{61}(nl_j) = \frac{32}{3} \frac{1(l+1)}{n^2} \sum_{m=1}^{\infty} \frac{1}{(2l+m)} \quad (l \geq 2); \quad (11c)$$

For given orbital angular momentum l , the coefficient A_{61} approaches a constant as $n \rightarrow \infty$. Equation (11c) implies that A_{61} is spin-independent for $l \geq 2$, i.e., for D, F, G, ... states. Therefore, A_{61} does not contribute to the fine structure of these states.

III. THE METHOD

In this section, we illustrate the usefulness of the so-called method [10, 12, 13] in bound-state calculations. It is known that higher-order terms in the expansion of the bound-electron propagator in powers of Coulomb vertices and relativistic corrections to the wavefunction generate terms of higher order in Z^{-1} (see, e.g., Ref. [42] and references therein); these terms manifest themselves in Eq. (5) in the form of the function $G_{SE}(nl_j; Z)$, which summarizes these effects at the order of $(Z)^{-6}$. It is also well known that for very soft virtual photons, the potential expansion fails and generates an infrared divergence, which is cut off by the atomic momentum scale, Z^{-1} (see, e.g., Ref. [42] and references therein). This cutoff for the infrared divergence is one of the mechanisms that lead to the logarithmic terms in Eq. (5).

The method is used for the separation of the two different energy scales for virtual photons: the nonrelativistic domain, in which the virtual photon assumes values of the order of the atomic binding energy, and the relativistic domain, in which the virtual photon assumes values of the order of the electron rest mass. We consider here a model problem with one "virtual photon," that involves the separation of the function being integrated into a high- and a low-energy contribution. This necessitates the temporary introduction of a parameter ω ; the dependence on ω will cancel at the end of calculation [see Eq. (22) below] when the high- and the low-energy parts are added together. We have,

$$\begin{array}{ll} \text{nonrelativistic domain} & \text{electron rest mass,} \\ \text{i.e., } (Z)^{-2} m & m; \end{array} \quad (12)$$

The high-energy part is associated with photon energies $\omega > m$, and the low-energy part is associated with photon energies $\omega < m$.

In order to illustrate the principles behind the procedure, we discuss a simple, one-dimensional example: the evaluation of

$$J(Z) = \int_0^Z \frac{(Z')^2}{(Z')^2 + 1} \frac{1}{1 - Z'^2} dZ'; \quad (13)$$

where the integration variable Z' may be interpreted as the "energy" of a "virtual photon." The integral J can be explicitly calculated, so that the perturbation expansion can be checked:

$$J(Z) = \frac{1}{2} + \frac{2(Z)^2 \ln \frac{1}{(Z)^2} + 1}{\frac{1}{1 - (Z)^2}}; \quad (14)$$

For $|Z| < 1$, this formula is uniquely defined; the analytic continuations of the logarithm and of the square-root have to be performed consistently with the original definition (13).

Within the ϵ method, we start by dividing the calculation of $J(Z)$ into a high-energy part $J_H(Z; \epsilon)$ and a low-energy part $J_L(Z; \epsilon)$, each of which depends on an additional parameter ϵ [that satisfies (12)]. The sum of the high- and low-energy contributions, which is

$$J(Z) = J_H(Z; \epsilon) + J_L(Z; \epsilon); \quad (15)$$

does not depend on ϵ . Therefore, the dependence on ϵ should vanish entirely when we add the high- and low-energy contributions. We may therefore expand both contributions J_H and J_L first in Z , then in ϵ , and then add them up at the end of the calculation in order to obtain the semi-analytic expansion of $J(Z)$ in powers of Z and $\ln(Z)$.

Let us first discuss the "high-energy part" of the calculation. It is given by the expression

$$J_H(Z; \epsilon) = \int_0^Z \frac{(Z')^2}{(Z')^2 + 1} \frac{1}{1 - Z'^2} dZ'; \quad (16)$$

where it is important to note in particular the lower integration limit, ϵ . For $\epsilon > 0$, we may expand

$$\frac{(Z')^2}{(Z')^2 + 1} = 1 - \frac{2(Z')^2}{1 + (Z')^2} + O[(Z')^4]; \quad (17)$$

Each corresponding term of (16) can be integrated, with result

$$J_H(Z; \epsilon) = \frac{1}{2} + \dots + 2(Z)^2 \ln \frac{2}{\epsilon} + \dots + O[(Z)^4]; \quad (18)$$

where the ellipsis represent terms that vanish as $\epsilon \rightarrow 0$. It is sufficient to only include terms that don't vanish as $\epsilon \rightarrow 0$, to each order in Z , because the sum J in Eq. (15) does not depend on ϵ . Moreover, this makes the calculation more manageable. The full cancellation of

the dependence on $\ln \epsilon$ will be explicit after we evaluate the "low-energy part."

The contribution of the low-energy part ($0 < \epsilon < 1$) reads

$$J_L(Z; \epsilon) = \int_0^Z \frac{(Z')^2}{(Z')^2 + 1} \frac{1}{1 - Z'^2} dZ'; \quad (19)$$

where the upper limit of integration depends on ϵ . For $\epsilon < 1$, we use an expansion that avoids the infrared divergences that we encountered in Eq. (17):

$$\frac{1}{1 - Z'^2} = 1 + \frac{Z'^2}{2} + \frac{3}{8} Z'^4 + \dots; \quad (20)$$

which leads to a Z expansion of the low-energy part. We obtain for J_L :

$$J_L(Z; \epsilon) = \frac{1}{2} + 2(Z)^2 \ln \frac{1}{(Z)^2} + \dots + O[(Z)^4 \ln^j(Z)]; \quad (21)$$

where the ellipsis again represent terms that vanish as $\epsilon \rightarrow 0$, and where j is some integer.

When the high-energy part (18) and the low-energy part (21) are added, the logarithmic divergences in ϵ cancel, as it should, and we have

$$\begin{aligned} J(Z) &= J_H(Z; \epsilon) + J_L(Z; \epsilon) \\ &= \frac{1}{2} + 2(Z)^2 \ln[(Z)^2] + \ln 2 \\ &\quad + O[(Z)^4 \ln^j(Z)] \end{aligned} \quad (22)$$

(for some j). We note the analogy of the above expression with the leading-order terms of the Z expansion of the function $F(n, j; Z)$ given in Eq. (7) for $l \neq 0$ (terms associated to the coefficients A_{40} , A_{61} , and A_{60}). In an actual Lamb shift calculation, the simplifications observed between terms containing ϵ are crucial [2, 13].

In this model example, the ϵ method allowed us to obtain (22) with minimal effort. For comparison, the reader may consider App. A of [43], which illustrates the cancellation of ϵ in higher orders of the Z expansion, using a different example.

IV. CALCULATION OF SELF-ENERGY COEFFICIENTS

This section, along with the previous one, gives detail on the methods we used in order to obtain the values of the A_{60} coefficient in Tables I-IV (see also Ref. [8]). The purpose of our calculations is to provide data for the self-energy coefficients up to and including the relative order $(Z)^2$ [see Eq. (7)]; for the states of interest here (non-S states) this corresponds to the coefficients A_{40} , A_{61} and A_{60} . Equation (8) is the well-known general formula for the coefficient A_{40} . The coefficient A_{61}

can be found in Eq. (10), with special cases treated in Eqs. (11a)-(11c). The remaining nonlogarithmic term A_{60} is by far the most difficult to evaluate, and the first results for any with orbital angular momentum quantum number $l \geq 2$ were recently obtained in Ref. [8] by using the methods described in this section.

As explained in detail in [10, 12, 13], the calculation of the one-loop selfenergy falls naturally into a high- and a low-energy part (F_H and F_L , respectively). In Sec. III, we illustrated this procedure, and the introduction of the scale-separation parameter μ for the photon energy. According to [12, Eqs. (39)-(43)], the contributions to the low-energy part can be separated naturally into the nonrelativistic dipole and the nonrelativistic quadrupole part, and into relativistic corrections to the current, to the Hamiltonian, to the binding energy and to the wavefunction of the bound state. We follow here the approach outlined in Refs. [12, 13], with some modifications.

One main difference as compared to the evaluation scheme described previously concerns the nonrelativistic quadrupole (nq) part. It is given by a specific matrix element (see the definition of P_{nq} in Ref. [12, Eq. (39)]), which has to be evaluated on the atomic state and averaged over the angles of the photon wave vectors:

$$\begin{aligned} \sum_{\mathbf{k}} \frac{d_{\mathbf{k}}}{4} P_{nq} &= \sum_{\mathbf{k}} \frac{d_{\mathbf{k}}}{4} \frac{T_{ij}}{6m} \\ &= p^i e^{i\mathbf{k} \cdot \mathbf{r}} \frac{1}{H_S} \frac{1}{(E - \epsilon)^2} p^j e^{i\mathbf{k} \cdot \mathbf{r}} \\ &= p^i \frac{1}{H_S} \frac{1}{(E - \epsilon)^2} p^j \end{aligned} \quad (23)$$

where the transverse function is given by

$$T_{ij} = \epsilon_{ij} \frac{k^i k^j}{k^2}.$$

The dipole interaction obtained by the replacement

$$\exp(i\mathbf{k} \cdot \mathbf{r}) \rightarrow 1$$

is subtracted; it leads to a lower-order contribution. The next term in the Taylor expansion of the exponential reads

$$\sum_{\mathbf{k}} \frac{d_{\mathbf{k}}}{4} \frac{T_{ij}}{6m} \quad (24)$$

$$\begin{aligned} &= p^i(\mathbf{k} \cdot \mathbf{r}) \frac{1}{H_S} \frac{1}{(E - \epsilon)^2} p^j(\mathbf{k} \cdot \mathbf{r}) \\ &= p^i \frac{1}{H_S} \frac{1}{(E - \epsilon)^2} p^j(\mathbf{k} \cdot \mathbf{r}^2) \quad : \end{aligned}$$

This representation makes an evaluation in coordinate space possible. However, an evaluation of this expression leads to a rather involved angular momentum algebra.

Specifically, we employ a well-known angular momentum decomposition of the coordinate-space hydrogen Green function [44]

$$G(\mathbf{r}_1; \mathbf{r}_2; E - \epsilon) = \sum_{l^0, m^0} g_{l^0}(\mathbf{r}_1; \mathbf{r}_2; E - \epsilon) Y_{l^0, m^0}(\hat{\mathbf{r}}_1) Y_{l^0, m^0}(\hat{\mathbf{r}}_2); \quad (25)$$

with $E - \epsilon = \epsilon - 2m = (Z^2)^{-1}$, and [45]

$$\begin{aligned} g_{l^0}(\mathbf{r}_1; \mathbf{r}_2; E - \epsilon) &= \frac{4m}{a} \frac{2r_1}{a} \frac{1^{l^0}}{a} \frac{2r_2}{a} \frac{1^{l^0}}{a} e^{-(r_1 + r_2)/a} \\ &= \sum_{k=0}^{l^0} \frac{L_k^{2l^0+1} \frac{2r_1}{a} L_k^{2l^0+1} \frac{2r_2}{a}}{(k+1)_{2l^0+1} (l^0+1+k)}; \end{aligned} \quad (26)$$

where $a = 1/(Zm)$, $(k)_c$ is the Pochhammer symbol, and L denotes associated Laguerre polynomials [41]. For a reference state $|j\rangle$ of angular momentum l , we obtain in (24) nonzero contributions from Green-function components (25) with $l^0 = l - 2; l - 1; l + 1; l + 2$. These can be obtained by straightforward, but tedious application of angular momentum algebra (see, e.g., [46]).

As in previous calculations (see also [12, Eqs. (18) and (19)] and [13, Eqs. (55)-(58)]), we obtain for the high-energy part of all atomic states the general structure

$$\begin{aligned} F_H(n_l; Z) &= \frac{1}{2} \frac{1}{(2l+1)} \\ &+ (Z)^2 K \frac{C}{A_{61}} \ln(Z) + O(\epsilon) \\ &+ \dots \end{aligned} \quad (27)$$

where K is a constant, and where the ellipsis denotes higher-order terms [in Z and $\ln(Z)$]. As observed in Sec. III, we may suppress terms that vanish in the limit $\epsilon \rightarrow 0$ [terms of the form $O(\epsilon)$ in the $(Z)^2$ -term in Eq. (27) above]. These terms cancel when the high- and low-energy parts are added.

Together with the constant term $A_{61} \ln 2$, the constant K contributes to A_{60} . C is the coefficient of the $1/\epsilon$ divergence; the term $C =$ cancels when the high- and low-energy parts are added. Both K and C are state dependent and vary with $n; j; l$. As in [12, Eqs. (56) and (57)] and [13, Eqs. (89)-(92)], the low-energy part, for all states under investigation, has the general structure:

$$\begin{aligned} F_L(n_l; Z) &= \frac{4}{3} \ln k_0(n_l) \\ &+ (Z)^2 L + \frac{C}{(Z)^2} + A_{61} \ln \frac{1}{(Z)^2} + O(\epsilon) \\ &+ \dots \end{aligned} \quad (28)$$

where $\ln k_0(n_l)$ is the Bethe logarithm [see Eq. (9)], and where the ellipsis denotes higher-order terms. The cancellation of the divergence in between (27) and (28) is obvious. The constant L , which is state-dependent (a

function of $n; j; l$), represents the low-energy contribution to A_{60} and can be interpreted as the relativistic generalization of the Bethe logarithm. In terms of the general expressions (27) and (28), A_{60} is therefore given by

$$A_{60} = K A_{61} \ln 2 + L; \quad (29)$$

Our improved results for A_{60} coefficients rely essentially on a more general code for the analytic calculations, written in the computer-algebra package Mathematica [47, 48], which enables the corrections to be evaluated semi-automatically. Intermediate expressions with some 200,000 terms are encountered, and the complexity of the calculations sharply increases with the principal quantum number n , and, as far as the complexity of the angular momentum algebra is concerned, with the orbital angular quantum number of the bound electron.

Of crucial importance was the development of convergence acceleration methods which were used extensively for the evaluation of remaining one-dimensional integrals which could not be done analytically. These integrals are analogous to expressions encountered in previous work (see [12, Eqs. (36), (47) and (48)] and [13, Eqs. (80)–(84)]). The numerically evaluated contributions involve slowly convergent hypergeometric series, and in more extreme cases infinite series over partial derivatives of hypergeometric functions, and generalizations of Lerch's transcendent [49, 50]. As a result of the summation over l^0 in (25), after performing radial integrals, two specific hypergeometric functions enter naturally into the expressions for the bound-state matrix elements that characterize the one-loop correction (see, e.g., [13, Eqs. (80) and (81)]. One of these functions is given by

$${}_1(n;t) = {}_2F_1\left(1; nt; 1 - nt; \frac{1-t}{1+t}\right); \quad (30)$$

where the integration variable t is in the range $0 < t < 1$, and n is the bound-state principal quantum number. For $t \rightarrow 0$, the power series expansion of ${}_1$ is slowly convergent,

$${}_1(n;t) = (nt)^{\sum_{k=0}^{\infty} \frac{1-t}{1+t} 2k}{nt - k}; \quad (31)$$

The series is nonalternating. In order to accelerate the convergence in the range $t \in (0; 0.05)$, we employ the combined nonlinear-condensation transformation [6, 27]. The other hypergeometric function that occurs naturally in our calculations is

$${}_2(n;t) = {}_2F_1\left(1; nt; 1 - nt; \frac{1-t}{1+t}\right); \quad (32)$$

For $0 < t < 0.05$, we accelerate the convergence of the alternating power series

$${}_2(n;t) = (nt)^{\sum_{k=0}^{\infty} \frac{1-t}{1+t} k}{nt - k}; \quad (33)$$

TABLE I: Self-energy coefficient A_{60} (6) for P states [see Eq. (7)]. The quoted error is due to numerical integration. As in previous calculations (see Refs. [12, 13]), certain remaining one-dimensional integrals involving (partial derivatives of) hypergeometric functions could only be evaluated numerically.

n	$P_{1=2} (\ell = 1)$	$P_{3=2} (\ell = 2)$
2	0:998 904 402 (1)	0:503 373 465 (1)
3	1:148 189 956 (1)	0:597 569 388 (1)
4	1:195 688 142 (1)	0:630 945 795 (1)
5	1:216 224 512 (1)	0:647 013 508 (1)
6	1:226 702 391 (1)	0:656 154 893 (1)
7	1:232 715 957 (1)	0:662 027 568 (1)

TABLE II: A_{60} coefficients (6) for D states.

n	$D_{3=2} (\ell = 2)$	$D_{5=2} (\ell = 3)$
3	0:005 551 573 (1)	0:027 609 989 (1)
4	0:005 585 985 (1)	0:031 411 862 (1)
5	0:006 152 175 (1)	0:033 077 570 (1)
6	0:006 749 745 (1)	0:033 908 493 (1)
7	0:007 277 403 (1)	0:034 355 926 (1)
8	0:007 723 850 (1)	0:034 607 492 (1)

via the transformation [51, Eq. (8.4-4)]. The convergence acceleration leads to a much more reliable evaluation of the remaining numerical integrals which contribute to A_{60} (but cannot be expressed in closed analytic form). As a by-product of our investigations, we obtain Bethe logarithms with increased precision. Here, we restrict the accuracy to 24 figures and give results for P states,

$$\begin{aligned} \ln k_0(2P) &= 0:030 016 708 630 212 902 443 676(1); \\ \ln k_0(3P) &= 0:038 190 229 385 312 447 701 163(1); \\ \ln k_0(4P) &= 0:041 954 894 598 085 548 671 037(1); \\ \ln k_0(5P) &= 0:044 034 695 591 877 795 070 318(1); \end{aligned} \quad (34)$$

These results are in agreement with other recent calculations [5, 39, 40].

The main results of this paper concerning the A_{60} coefficients are given in Tables I–IV, with an absolute pre-

TABLE III: A_{60} coefficients (6) for F states.

n	$F_{5=2} (\ell = 3)$	$F_{7=2} (\ell = 4)$
4	0:002 326 988 (1)	0:007 074 961 (1)
5	0:002 403 158 (1)	0:008 087 020 (1)

TABLE IV: A_{60} coefficients (6) for G states.

n	$G_{7=2}$ ($= 4$)	$G_{9=2}$ ($= 5$)
5	0:000 814 415 (1)	0:002 412 929 (1)

TABLE V: According to Eqs. (27) and (28), the high- and low-energy parts can be cast into a general form involving the terms C , K and L . The coefficient A_{60} can be expressed in terms of K , A_{61} and L according to (29). Here, we present analytic results for the terms C , A_{61} and K , and numerical results for L (for states with $n = 5$). The results for A_{61} can be inferred from Eqs. (10)-(11c). For $l = 2$, we observe that the A_{61} are spin-independent and that $C = A_{61}$.

C, K and L coefficients for states with $n = 5$				
state	C	A_{61}	K	L
5P ₁₌₂	$\frac{292}{1125}$	$\frac{796}{1125}$	$\frac{20129}{67500}$	1:023 991 781 (1)
5P ₃₌₂	$\frac{292}{1125}$	$\frac{436}{1125}$	$\frac{199387}{540000}$	0:747 615 653 (1)
5D ₃₌₂	$\frac{92}{7875}$	$\frac{92}{7875}$	$\frac{35947}{3780000}$	0:023 759 683 (1)
5D ₅₌₂	$\frac{92}{7875}$	$\frac{92}{7875}$	$\frac{3097}{157500}$	0:021 511 798 (1)
5F ₅₌₂	$\frac{2}{1125}$	$\frac{2}{1125}$	$\frac{2657}{1102500}$	0:006 045 397 (1)
5F ₇₌₂	$\frac{2}{1125}$	$\frac{2}{1125}$	$\frac{774121}{211680000}$	0:005 662 248 (1)
5G ₇₌₂	$\frac{2}{4725}$	$\frac{2}{4725}$	$\frac{4397}{6048000}$	0:001 834 827 (1)
5G ₉₌₂	$\frac{2}{4725}$	$\frac{2}{4725}$	$\frac{269}{283500}$	0:001 757 471 (1)

cision of 10^{-9} . In addition, we give explicit expressions for the low and high-energy parts of the self energy, for the states with $n = 5$ under investigation [see Eqs. (27) and (28) and Table V]. These may be helpful in an independent verification of our calculations. Note that the $G_{7=2}$ and $G_{9=2}$ states involve the most problematic angular momentum algebra of all atomic states considered here.

For some P states (see Table I), the values of A_{60} reported here are four orders of magnitude more accurate than previous results [12, 13], due to the improved numerical algorithms. For the 3P₁₌₂ states, the numerical value for the A_{60} coefficients of Table I differs from the previously reported result [13] by more than the numerical uncertainty quoted in Ref. [13], whereas they are in agreement with previous results [12, 13] in the case of 2P₁₌₂ and 4P₁₌₂ states. The discrepancy for A_{60} (3P₁₌₂) is on the level of $5 \cdot 10^4$ in absolute units, which corresponds to roughly 2 Hz in frequency units for atomic hydrogen. The computational error in Ref. [13] was caused by numerical difficulties in one of the remaining one-

dimensional integrals involving the hypergeometric functions (30) and (32), which could not be evaluated analytically. The numerical difficulties encountered in previous calculations due to slow convergence of the integrals are essentially removed by the convergence acceleration techniques.

Contributions to the low-energy part (5G ₇₌₂)	
A_{60} -contribution due to F_{nq}	0:002 875 830 9 (5)
A_{60} -contribution due to F_y	0:001 083 109 4 (5)
A_{60} -contribution due to F_H	0:008 917 782 1 (5)
A_{60} -contribution due to F_E	0:004 920 556 0 (5)
A_{60} -contribution due to F	0:004 039 332 1 (5)
A_{60} (see entry for L in Table V)	0:001 834 827 (1)

TABLE VII: For the 5G₇₌₂ state, an additional numerical cancellation occurs when the finite contributions to A_{60} originating from the low-energy part (see the ninth row of Table V) and the high-energy part are added according to Eq. (29). The high-energy contribution is $A_{60}(F_H) = K A_{61} \ln 2$, and the low-energy contribution is $A_{60}(F_L) = L$.

$A_{60}(F_H)$	0:001 020 413
$A_{60}(F_L)$	0:001 834 828 (1)
A_{60}	0:000 814 415 (1)

dimensional integrals involving the hypergeometric functions (30) and (32), which could not be evaluated analytically. The numerical difficulties encountered in previous calculations due to slow convergence of the integrals are essentially removed by the convergence acceleration techniques.

For some states, rather severe numerical cancellations are observed between the high- and low-energy contributions to the self energy as well as between the different contributions to the low-energy part. This intriguing observation is documented in Tables VI and VII, using the 5G₇₌₂ state as an example. Note that these numerical cancellations go beyond the required exact, analytic cancellation of the divergent contributions which depend on the scale-separation parameter λ .

V. A_{60} FOR HIGHER- n STATES

This section contains approximate formulas that we have found for the A_{60} coefficients of P and D states, for principal quantum numbers n that go beyond those of Tables I and II. These tables contain enough values of $A_{60}(n, l_j)$ for extrapolations to be made. We present

TABLE V III: The asymptotic behavior of $A_{60}(n l_j)$ as $n \rightarrow \infty$ can be described by an expansion in $1/n$. The following table contains the first coefficients of such an expansion, as defined in Eq. (35). The approximate values of $A_{60}(n l_j)$ that can be directly deduced from this table and from Eq. (35b) are the best available values of A_{60} for P and D states, except for the states that are represented in Tables I and II. These results are depicted in Fig. 1.

state	a_0	a_1	a_2
$P_{1=2}$	1.249 (9)	0.0 (2)	0.07 (45)
$P_{3=2}$	0.69 (2)	0.15 (5)	0.25 (25)
$D_{3=2}$	0.011 (1)	0.032 (7)	0.05 (9)
$D_{5=2}$	0.034 (2)	0.025 (5)	0.18 (4)

the asymptotic behavior of $A_{60}(n l_j)$ as $n \rightarrow \infty$ as

$$A_{60}(n l_j) = A_3(n; l_j) + O\left(\frac{1}{n^3}\right); \quad (35a)$$

where

$$A_3(n; l_j) = a_0(l_j) + \frac{a_1(l_j)}{n} + \frac{a_2(l_j)}{n^2}; \quad (35b)$$

Such an asymptotic behavior is justified, for any non-S state, by its similarity to the functional form of the self-energy coefficient A_{61} in Eq. (7) [see Eq. (11)]. The values that we obtained for the coefficients $a_i(l_j)$ can be found in Table V III. The fitting method is described in the Appendix.

The approximation $A_3(n; l_j)$ to $A_{60}(n l_j)$ is depicted in Fig. 1, for P and D states. According to the graphs in this figure, the $O(1/n^3)$ contribution in (35a) is much smaller than the uncertainty in A_3 , which comes from the uncertainties in the coefficients of Table V III. As can be seen in Fig. 1, the coefficients provided in Table V III also yield approximate values of A_{60} which are valid for any principal quantum number n (for P and D states).

The coefficients a_i of (35b) given in Table V III can be useful to spectroscopy experiments that involve electronic levels with principal quantum numbers that are higher than those of Tables I and II. In fact, the self energy of the electron of an hydrogenlike ion can be estimated through Eqs. (7), (8), (11) and (35), with A_3 defined with the values of Table V III. Hydrogen has been and will be the subject of extremely precise spectroscopy experiments, which now reach the level of 1 Hz of uncertainty in transition frequencies. The uncertainty in the self energy (Δ) that comes from the uncertainties of the coefficients of Table V III through (7) and (35) is comparable to the current experimental limit. In fact, the uncertainties on A_3 in (35b) contribute to the self energy by less than 2 Hz for $P_{1=2}$ states with $n > 7$, less than 1.6 Hz for $P_{3=2}$ states with $n > 7$, less than 0.12 Hz for $D_{5=2}$ states with $n > 8$, and less than 0.12 Hz for $D_{5=2}$ states with $n > 8$.

Moreover, the coefficients of Table V III can be useful to theoretical calculations. In fact, future values of A_{60}

for P and D states can be checked against the estimates provided by A_3 in (35b) [see also the curves of Fig. 1.

VI. APPROXIMATIONS OF A_{60} AND OF THE BETHE LOGARITHM

In addition to studying the dependence of $A_{60}(n l_j)$ on n , as we did in the previous section for P and D states, it is interesting to analyze the behavior of $A_{60}(n l_j)$ as a function of l , for $j = 1$ and $j = 1 + 1 = 2$. We conjecture that $A_{60}(n l_j)$, for $n = l + 1$ and $j = 1$ and $j = 1 + 1 = 2$, decreases as

$$A_{60}(n l_j) \sim \frac{c(j-1)}{l^k} \quad \text{with } k \geq 3; \quad (36)$$

where we probably have $k = 4$ or $k = 5$ [$c(1=2)$ and $c(1=2)$ are two unspecified numbers]. The form (36) is motivated in this section.

We have also studied the asymptotic behavior of the Bethe logarithm $\ln k_0(n l)$, because this is a quantity similar to the "relativistic Bethe logarithm" A_{60} , and because it yields a large contribution to the self energy [see Eqs. (7) and (8)]. We show in this section that the Bethe logarithm $\ln[k_0(n l) = R_1]$, where $n = l + 1$, appears to behave asymptotically as $1/l^3$ (R_1 denotes the Rydberg constant). This result differs from the $1/l^{7=2}$ asymptotic behavior of $\ln[k_0(n l) = R_1]$ deduced from Eq. (B 5) in [52, p. 845]. Extrapolations of the Bethe logarithm $\ln k_0(n l)$ as a function of n were used in Ref. [53] for S, P and D states ($l = 0$ to 2).

We also postulate that the Bethe logarithm $\ln k_0(n l)$, where $n = l + 1$, can be expanded in powers of $1/l$ about $l = 1$. In order to find the first few coefficients of such an expansion, we used the fitting procedure described in the Appendix. The resulting approximation reads:

$$\begin{aligned} & l^3 \ln[k_0(n l) = R_1] \\ &= 0.056853(2) + \frac{0.02478(4)}{l} + \frac{0.0387(8)}{l^2} \\ &+ \frac{0.114(6)}{l^3} + \frac{0.16(2)}{l^4}; \end{aligned} \quad (37)$$

where $n = l + 1$, and where the neglected contribution is of order $1/l^5$. This approximation should be valid for $l \geq 1$; nevertheless, it yields values of the Bethe logarithm that are both precise (see Fig. 2) and compatible with all the values of $\ln[k_0(n l) = R_1]$ for $l = 3; \dots; 19$ (taken from Ref. [5]). For the $l \leq 20$ levels of hydrogen, the uncertainty in the result of approximation (37) is negligible, when compared to the best experimental uncertainty in frequency measurements (about 1 Hz [1]).

Moreover, we suggest that the orders of magnitude of the self-energy coefficient $A_{60}(n l_j)$ and of the Bethe logarithm $\ln k_0(n l)$ do not depend on the principal quantum number n , i.e., the order of magnitude of a coefficient $A_{60}(n l_j)$ is given by the order of magnitude

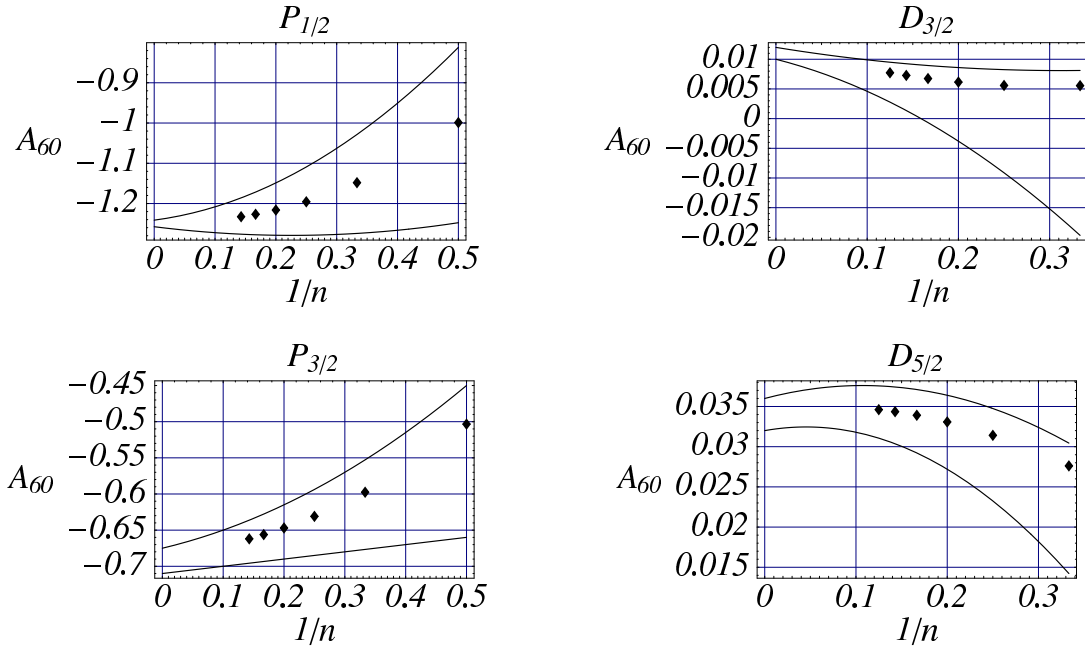


FIG. 1: These graphs show exact and approximate values of the selfenergy coefficient A_{60} | see Eq. (7). Exact values are represented by dots and can be found in Tables I and II. The two curves of each graph represent the upper and lower limits of the approximation to A_{60} provided by A_3 in Eqs. (35), by taking into account the uncertainties on the coefficients of Table V III. For levels in hydrogen with principal quantum number $n = 10$, the uncertainty in A_{60} deduced from these curves contribute to the uncertainty in the electron self energy (1) by less than 2 Hz.

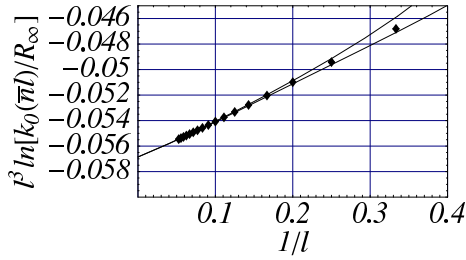


FIG. 2: Comparison between exact values of $l^3 \ln[k_0(nl)=R_1]$ (dots) and the truncated asymptotic expansion of Eq. (37) (zone between the two curves) | $\ln[k_0(nl)=R_1]$ is the Bethe logarithm, and $n = l+1$. The numerical values of the Bethe logarithms used in this graph [5] are compatible with the values deduced from Eq. (37), which are in the area between the two curves. The fact that the data points seem to converge toward a finite value (≈ -0.057) as $1/l \rightarrow 0$ supports the conjecture of a l^{-3} asymptotic behavior of the Bethe logarithm $\ln[k_0(nl)=R_1]$.

of $A_{60}(nl_j)$, where $n = l+1$ (and similarly for the Bethe logarithm). For A_{60} , this behavior is a generalization of what is observed for P, D, F and G states in Tables I{IV}. For the Bethe logarithm, the fact that $\ln k_0(nl)$ and $\ln k_0(nl)$ have the same order of magnitude can be observed for states with $l < n = 20$ by inspecting the results of Ref. [5].

The expressions (36) and (37) for the asymptotic behavior of $A_{60}(nl_j)$ and $\ln[k_0(nl)=R_1]$, where $n = l+1$,

could thus be used for estimating the order of magnitude of the selfenergy (1) | with the help of Eqs. (7), (8), (11). Estimating the selfenergy correction (1) can be useful in high-precision spectroscopy experiments with large- l levels. Thus, for instance, a recent experiment [7] required evaluating the selfenergies of circular ($n = l+1$) states of orbital quantum number $l' = 30$. On the theoretical side, future calculations of $A_{60}(nl_j)$ and $\ln[k_0(nl)=R_1]$ can be checked against the asymptotic behaviors of $A_{60}(nl_j)$ and $\ln[k_0(nl)=R_1]$ that are described above.

The order of magnitude of $A_{60}(nl_j)$ as a function of the orbital quantum number l (with either $j = l+1=2$ or $j = l-1=2$) is most naturally represented by the magnitude of either $\lim_{n \rightarrow \infty} A_{60}(nl_j)$ or $A_{60}(nl_j)$, where $n = l+1$ is the smallest n possible for a given l . We chose the latter possibility for two reasons. First, small- n values of $A_{60}(nl_j)$ are available (see Tables I{IV}). Second, future values of $A_{60}(nl_j)$ for higher angular quantum numbers l are likely to be obtained first for states where $n = l+1$, which is the smallest n possible for a given angular momentum quantum number l . In particular, such states have simpler radial wavefunctions (the number of terms in the radial wavefunction of a state increases with $n-l$). And finally, circular states ($n = l+1$) are relevant to high-precision spectroscopy experiments (see, e.g., Ref. [7]), whereas $n = 1$ states are unphysical.

As mentioned above, we expect an asymptotic behavior of the form l^{-k} , with k integer, for $A_{60}(nl_j)$ and for the Bethe logarithm $\ln[k_0(nl)=R_1]$. Such a functional form is motivated by the fact that all the $A_{ik}(nl_j)$ coefficients

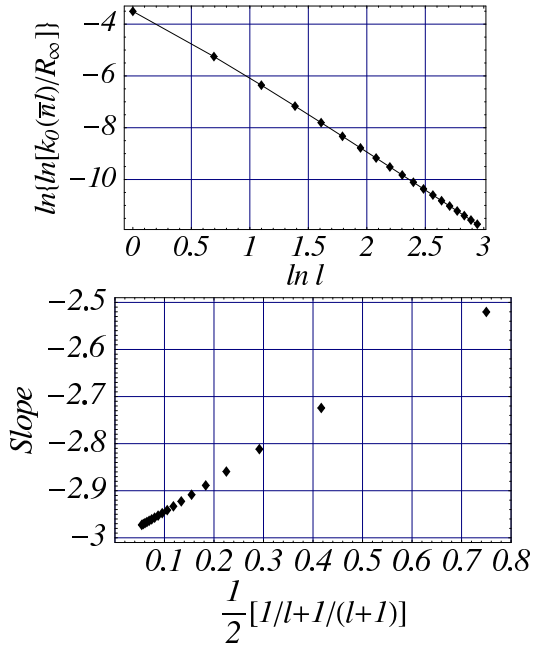


FIG. 3: Upper graph: log-log plot of the Bethe logarithm $\ln[k_0(n)=R_1]$, where $n = l+1$. Lower graph: slope between two successive points of the log-log plot. The limit slope of -3 as $l \rightarrow \infty$ observed in the lower graph indicates that the Bethe logarithm $\ln[k_0(n)=R_1]$ behaves asymptotically as l^{-3} . This confirms what is observed in Fig. 2.

coefficients of the selfenergy function F in Eq. (5) can be expanded in power series of $l=n$ and $l=l$, except maybe for the two coefficients related to this section, A_{60} and A_{40} , where the latter is a function of the Bethe logarithm [see Eq. (8)]. (We suppose that A_{60} and A_{40} can also be expanded in such a series.) This can for instance be checked with the formulas for $A_{ik}(n_l)$ reviewed in Ref. [2, p.468], with the help of Eq. (10) for $A_{61}(n_l)$, where $(n+1)$ can be expanded in powers of $l=(n+1)$ [41, x 6.3.18].

The l^{-3} behavior of the Bethe logarithm $\ln[k_0(n)=R_1]$, where $n = l+1$, is suggested by Fig. 2. The points of this graph, which represent

$$l^{-3} \ln[k_0(n)=R_1]; \quad (38)$$

appear to converge toward a limit (≈ 0.057) as $l \rightarrow \infty$. We checked the l^{-3} behavior deduced from the study of Eq. (38) by calculating the slope of a log-log plot of the Bethe logarithm $\ln[k_0(n)=R_1]$ (with numerical values taken from Ref. [5]). The result, shown in Fig. 3, indicates that the Bethe logarithm does indeed behave asymptotically as l^{-3} ; this coincides with the conclusion from Fig. 2.

It is possible to use the procedure depicted in Fig. 3 to estimate the integer exponent k of an asymptotic behavior l^{-k} for the relativistic Bethe logarithm $A_{60}(n_l)$, where $n = l+1$ and $j = l-1=2$. In fact, it is reasonable to use the Bethe logarithm $\ln[k_0(n)=R_1]$ as a guide for studying the relativistic Bethe logarithm A_{60} . Thus,

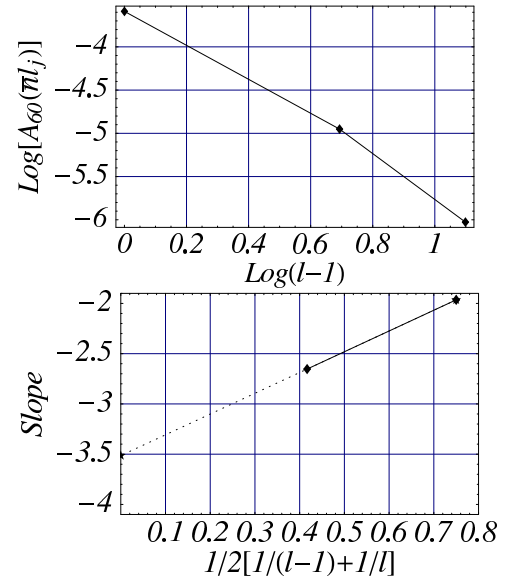


FIG. 4: Upper graph: log-log plot of the selfenergy coefficient $A_{60}(n_l)$, where $n = l+1$ and $j = l-1=2$. Lower graph: slope between two successive points of the log-log plot (solid line) and extrapolation to $l \rightarrow \infty$ (dashes). By analogy with the graphs similarly obtained for the Bethe logarithm in Fig. 3, we conclude that for $j = l-1=2$, $A_{60}(n_l)$ behaves asymptotically as l^{-k} with $k = 3$ and, probably, $k = 4$ or $k = 5$. The values of A_{60} are taken from Tables II(IV).

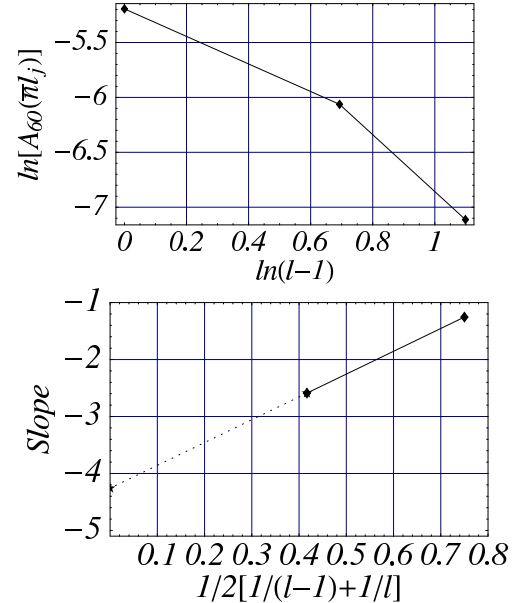


FIG. 5: Upper graph: log-log plot of the selfenergy coefficient $A_{60}(n_l)$, where $n = l+1$ and $j = l-1=2$. Lower graph: slope between two successive points of the log-log plot (solid line) and extrapolation to $l \rightarrow \infty$ (dashes). By analogy with the graphs similarly obtained for the Bethe logarithm in Fig. 3, we conclude that for $j = l-1=2$, $A_{60}(n_l)$ behaves asymptotically as l^{-k} with $k = 3$ and, probably, $k = 4$ or $k = 5$. The values of A_{60} are taken from Tables II(IV).

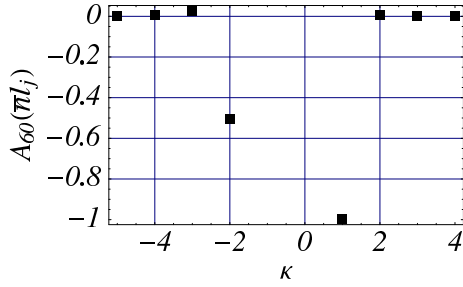


FIG. 6: This graph shows values of the self-energy coefficients $A_{60}(n_l_j)$, where $n = l + 1$, as a function of the Dirac quantum number k , where k is defined in (2). The large value $A_{60}(1S_{1=2}) \approx 31$ is not represented here. This plot shows that for S and P states ($l = 0, 1$ and 1), the A_{60} coefficient exhibits an exceptional behavior; such an exceptional behavior is also found in the self-energy coefficient A_{61} in Eq. (10), which is known analytically.

the procedure depicted in Fig. 3 was applied to the self-energy coefficient $A_{60}(n_l_j)$; we obtained the asymptotic behavior presented at the beginning of this section, and in particular in Eq. (36). The graphs supporting (36) are given in Fig. 4 for l with states with $j = l + 1 = 2$, and in Fig. 5 for states with $j = l - 1 = 2$. Each of these graphs uses only three values of A_{60} (D, F and G states); even though this is a relatively small number of values compared to the number of available values of the Bethe logarithm, the behavior of the first few data points in Fig. 3 justifies using only a few small- l values in order to predict the asymptotic behavior of $A_{60}(n_l_j)$ for $l \gg 1$.

The values of the A_{60} coefficient of S and P states were not used in obtaining Eq. (36), because it is convenient to treat the orders of magnitude of the A_{60} coefficient of these states separately from the orders of magnitude of higher- l states; Fig. 6 illustrates this point. We note that the self-energy coefficient A_{61} also exhibits an exceptional behavior for S and P states (see, e.g., Eq. (4.4a) in [3]). As a additional consequence, estimating the coefficient c of the asymptotic form of A_{60} in Eq. (36) would require use of states with orbital angular momentum quantum number $l \geq 2$ (D, F, etc.).

The possible values of the exponent k in Eq. (36) deduced from both the graphs of Fig. 4 and of Fig. 5 are compatible with each other ($k = 3$ with, probably, $k = 4$ or $k = 5$). It is indeed expected that the asymptotic form of $A_{60}(n_l_j)$ be the same for $j = l + 1 = 2$ and $j = l - 1 = 2$, as can be seen from the numerical values for D, F and G states found in Tables II{IV}. More precise estimates of the asymptotic exponent k in Eq. (36) can be obtained through the procedure we used in Figs. 4 and 5, as soon as additional values of $A_{60}(n_l_j)$, with $n = l + 1$ are available.

According to the results of this section, the relativistic Bethe logarithm $A_{60}(n_l_j)$ decreases at least as fast (and probably one or two powers faster), as a function of l , than the Bethe logarithm $\ln k_0(n_l)$. Such a behavior is also found in the Dirac-Coulomb energy of hydrogen

and hydrogenlike ions. Thus, the Dirac-Coulomb energy of an electron bound to a nucleus of charge number Z is (see, e.g., [2, p. 466])

$$E_{n,j} = 1 - \frac{(Z\alpha)^2}{(n-j)^2}; \quad (39)$$

where

$$= (j + 1 = 2) \frac{P}{(j + 1 = 2)^2 (Z\alpha)^2};$$

According to (39), an electron in a circular state n_l_j with $j = l + 1 = 2$ (and $n = l + 1$) has an energy

$$E_{n,l+\frac{1}{2}} = 1 - \frac{P}{(Z\alpha)^2 (l+1)^2}; \quad (40)$$

In the Taylor expansion (in $Z\alpha$) of this energy, the asymptotic behavior of the coefficient of $(Z\alpha)^{2k}$ is given by $1 = l^{2k}$ (this conclusion also holds for circular state n_l_j with $j = l - 1 = 2$). Thus, for circular states, successive relativistic corrections to the nonrelativistic energy of a bound electron fall off faster and faster with the orbital quantum number l , with two additional powers of $l = l$ for each order in $(Z\alpha)^2$. If this rule applies to the coefficients of the self-energy expansion (7), the asymptotic form of $A_{60}(n_l_j)$ as $l \rightarrow \infty$ should be $1 = l^4$; in fact, the lower-order coefficient $A_{40}(n_l_j)$ decreases as $1 = l^2$, as can be seen in Eq. (8). On the other hand, since $A_{60}(n_l_j)$ can be considered as a relativistic correction to the Bethe logarithm, applying the above rule yields an asymptotic form in $1 = l^5$ for $A_{60}(n_l_j)$, since the Bethe logarithm behaves as $1 = l^3$, as described in this section. These observations are fully compatible with the graphs of Figs. 4 and 5, from which the asymptotic form (36) of $A_{60}(n_l_j)$ was deduced (with an exponent k probably equal to 4 or 5).

VII. CHECKS OF THE A_{60} COEFFICIENTS

We have checked our analytic results for A_{60} (cf. Tables I{IV}) by an independent method: the analytic results were compared to values deduced from non-perturbative, numerical calculations of the self-energy (1). We have used the numerical self-energy values of Refs. [14, 22, 26, 54, 55, 56], as well as new values [57], which extend the results of Ref. [26] to smaller nuclear charge numbers Z (to Z between 10 and 25). In most cases, the checks that we detail below confirm the values of A_{60} reported in Tables I{IV}, to a relative precision of about 15%. The few exceptions are the following. For 2P states, the numerical values of the self-energy confirm the results of Table I to about 1%. For $nD_{3=2}$ states with $n = 3; \dots; 8$, the non-perturbative self-energy results yield $A_{60}(nD_{3=2}) = 0.005(10)$, in agreement with the results of Table II. And finally, we did not check $A_{60}(8D_{5=2})$ in Table II by using non-perturbative self-energy values because no such values are available for the $8D_{5=2}$ state. However, as depicted in Fig. 1, the value of

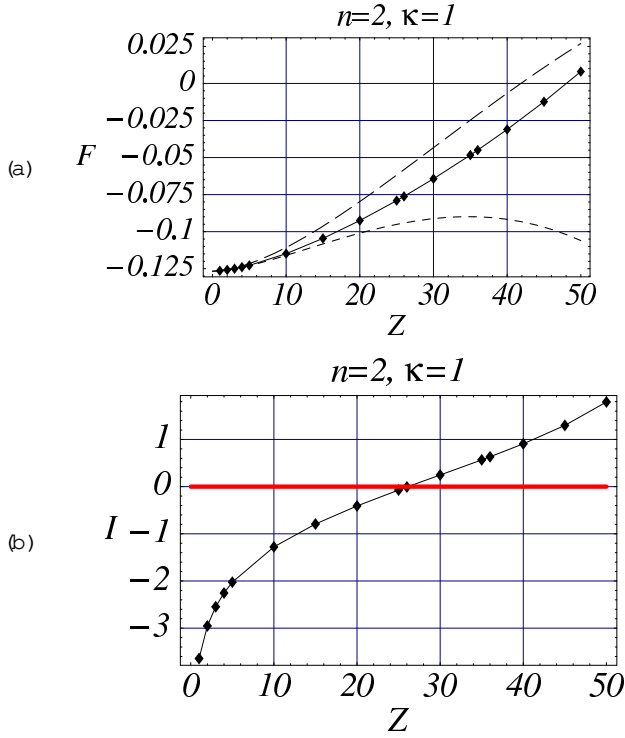


FIG. 7: Figure (a) shows exact and approximate values of the (scaled) self energy F of a $2P_{1=2}$ electron [see Eq. (1)]. Exact values are given on the solid line. The two-coefficient approximation (41) is represented by long dashes. The three-coefficient approximation (42) uses the value of $A_{60}(2P_{1=2})$ that we provide in Table I, and is indicated by short dashes. Figure (b) displays the improvement provided by the inclusion of A_{60} in the self-energy approximation, as measured by the function I in Eq. (43); negative values of I indicate that including A_{60} improves the approximation.

$A_{60}(8D_{5=2})$ reported here appears to fit well within the series of $A_{60}(nD_{5=2})$ values for $n = 3; \dots; 7$ (see Table II).

The first check that we applied consisted of comparing the numerical, exact results for F to two of its successive approximations. The first approximation, $F^{(2)}(Z)$, includes the two dominant and already-known coefficients A_{40} (8) and A_{61} (10) of expansion (7):

$$F^{(2)}(Z) = A_{40} + (Z)^2 A_{61} \ln(Z)^2; \quad (41)$$

and the second approximation, $F^{(3)}$, includes in addition the next-order contribution reported in this paper:

$$F^{(3)}(Z) = A_{40} + (Z)^2 A_{61} \ln(Z)^2 + A_{60}; \quad (42)$$

For a given electronic level $n l_j$, one expects that for low Z , the curve of the higher-order approximation $F^{(3)}(Z)$ be closer to the curve of $F(Z)$ than $F^{(2)}(Z)$. In order to check this, we plotted the quantity

$$I(Z) = \ln \frac{F(Z) - F^{(3)}(Z)}{F(Z) - F^{(2)}(Z)}; \quad (43)$$

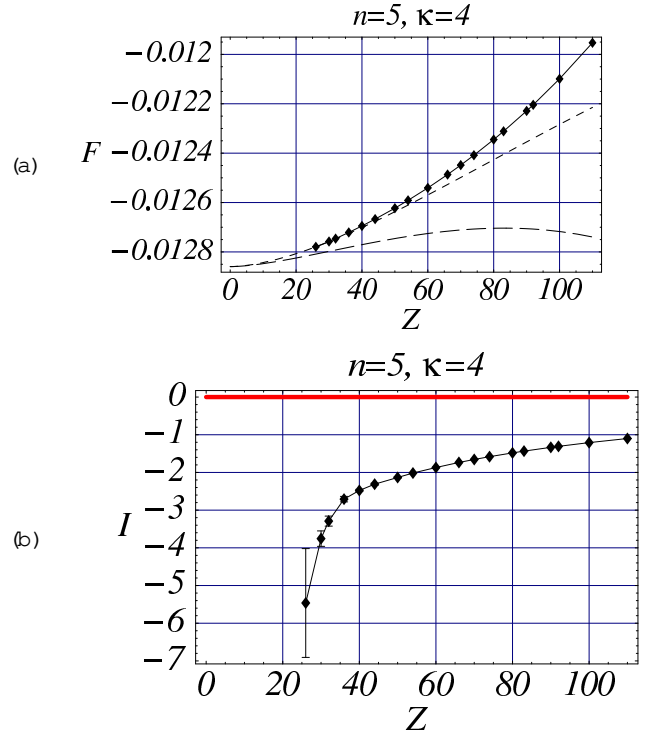


FIG. 8: These two figures represent respectively the same quantities as those found in Fig. 7, but for the $5G_{7=2}$ level instead of the $2P_{1=2}$ level. The fact that curve (b) contains negative values of I [see Eq. (43)] indicates that the three-order approximation (42) to the self energy (7) is better than the two-order approximation (41), at least over the range of nuclear charge numbers $Z = 25 \{110$. The three-order approximation (42) uses the value of $A_{60}(5G_{7=2})$ reported in Table IV.

which should go to -1 as $Z \rightarrow 0$, as can be seen from Eq. (7). In (43), the purpose of the logarithm is only to obtain more legible graphs; a value of I lower than zero indicates that including A_{60} in the approximation of F improves the lower-order approximation. For the states of Tables I{IV, graphs of (43) are compatible with their expected behavior [$I(Z)$ is negative for Z sufficiently close to zero, and is consistent with a -1 limit]. Figures 7 and 8 show this behavior for two electronic states.

Moreover, the improvement provided by the inclusion of A_{60} in the approximation for F becomes greater as the total angular momentum j increases: for given n and Z , the improvement function (43) decreases as j increases; this behavior is shown in Figs. 7 and 8. Similarly, the range of Z for which approximation $F^{(3)}$ is better than $F^{(2)}$ increases with increasing j . In the worst of the cases considered here ($j = 1=2$), approximation $F^{(3)}$ is better than $F^{(2)}$ up to $Z \approx 25$. As shown in Fig. 8, for a high- j level such as $5G_{7=2}$, the higher-order approximation $F^{(3)}$ is better than $F^{(2)}$ even up to $Z = 110$.

The second check consisted in estimating A_{60} from the numerical values of the self energy (1). For all the electronic levels $n l_j$ studied here, we have plotted the

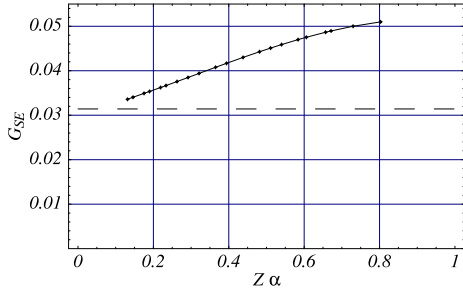


FIG. 9: Plot (solid line) of numerical values of the remainder $G_{SE}(4D_{5=2}; Z)$ of the self energy (5); the dashed line indicates the value of $A_{60}(4D_{5=2})$ reported in this paper (see Table II). By definition, the coefficient A_{60} can be obtained as the limit (6) of G_{SE} as $Z \rightarrow 0$. This plot shows that the value of A_{60} extracted from numerical self-energies is consistent with the value obtained by the calculations presented in this paper. We made identical observations for all the states of Tables I{IV}.

function $G_{SE}(n_l; Z)$ of (5); this is made possible by the fact that all the coefficients of (5) are known for all states [3, 28], except for A_{60} , which has been evaluated for a few states that include the ones we consider here [5, 39, 40]. As indicated in (6), the limit of the remainder $G_{SE}(n_l; Z)$ as $Z \rightarrow 0$ is by definition $A_{60}(n_l)$. We have estimated this limit both visually and by fitting $G_{SE}(n_l; Z)$ with various choices of non-zero higher-order terms. A typical curve for $G_{SE}(Z)$ is shown in Fig. 9. The estimates of A_{60} obtained by these procedures confirm the independent analytic results of Tables I{IV} to a typical accuracy of 10{20%, with a few exceptions. Thus, for 2P levels, plotting G_{SE} as in Fig. 9 allowed us to confirm the values of $A_{60}(2P_j)$ in Table I to a precision of about 1%. This exception comes from the fact that the self-energy of 2P states is known to high precision [14] for values of Z close to zero ($Z = 1; \dots; 5$): such values are well-suited to an evaluation of A_{60} by the limit (6). Plotting G_{SE} for $D_{3=2}$ states leads to $A_{60}(nD_{3=2}) = 0.005(10)$ for $n = 3; \dots; 8$, in agreement with Table II. Finally, since no non-perturbative self-energy (1) is available for $8D_{5=2}$ states, we were not able to independently obtain $A_{60}(8D_{5=2})$ by using such values.

As a by-product of our work with graphs of $G_{SE}(n_l; Z)$, we estimate the self-energy remainder $G_{SE}(n_l;)$ relevant to hydrogen ($Z = 1$) to be 0.030(5) for $3D_{5=2}$ and $4D_{5=2}$ states [see Eq. (5)]; this is larger than the estimate of 0.00(1) given in Ref. [2, p. 468]. These two new values change the previous estimate of the self-energy of $3D_{5=2}$ and $4D_{5=2}$ states through Eq. (7) by a relatively large amount, compared to the current best experimental uncertainty in transition frequencies (about 1 Hz [1]). Thus, a variation of 0.03 in $G_{SE}(3D_{5=2};)$ in (5) corresponds to a variation of about 50 Hz in the self-energy correction (1) of the $3D_{5=2}$ level in hydrogen. The same variation in $G_{SE}(4D_{5=2};)$ induces a variation of about 20 Hz in the self-energy of the $4D_{5=2}$ level in hydrogen; on the other hand, this latter change is small compared to

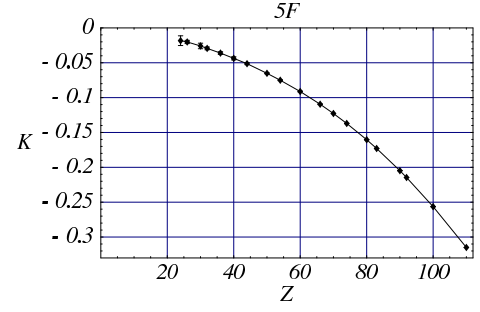


FIG. 10: Plot of the function K in Eq. (47) for the $5F_{7=2}$ and $5F_{5=2}$ states. The limit of this function as $Z \rightarrow 0$ must be zero if the coefficients A_{60} of Tables I{IV} agree with exact, numerical values of the self-energy. The curve displayed here indicates that the two values of ${}_{fs}A_{60}(5F)$ in Eq. (46) obtained independently from Table III and from non-perturbative self-energies (1) [via Eqs. (7), (8), (11c), (44) and (45)] do not differ by more than about 3%.

the uncertainty of the relevant measurements considered in Ref. [2].

As a third and last check, we used the numerical, exact values of F in order to study the following difference between remainders G_{SE} [see Eqs. (5) and (7)]:

$${}_{fs}G_{SE}(n_l; Z) = G_{SE}(n_{l+1=2}; Z) - G_{SE}(n_{l-1=2}; Z); \quad (44)$$

where, by definition of A_{60} (6),

$$\begin{aligned} \lim_{Z \rightarrow 0} {}_{fs}G_{SE}(n_l; Z) &= A_{60}(n_{l+1=2}) - A_{60}(n_{l-1=2}) \\ &= {}_{fs}A_{60}(n_l); \end{aligned} \quad (45)$$

which denotes a quantity associated to the n -structure. The numerical evaluation of this limit is interesting: for the states of Tables I{IV}, the numerical results for F yield values of ${}_{fs}A_{60}(n_l)$ that are more accurate than our numerical estimates of the two individual terms $A_{60}(n_{l+1=2})$ and $A_{60}(n_{l-1=2})$. Our analytic values for ${}_{fs}A_{60}$ in Eq. (46) were checked by plotting

$$K(Z) = \frac{{}_{fs}G_{SE}(n_l; Z)}{{}_{fs}A_{60}(n_l)} - 1; \quad (47)$$

where ${}_{fs}G_{SE}(n_l; Z)$ was calculated from the numerical values of F [see Eq. (7) and the coefficients reproduced in Sec. II], and where the value of ${}_{fs}A_{60}(n_l)$ in Eq. (46) was deduced from the analytic results of Tables I{IV}. If the numerical and analytic estimates of ${}_{fs}A_{60}(n_l)$ do agree, the function (47) goes to zero as $Z \rightarrow 0$. This is indeed consistent with what we observed; figure 10 provides an example of this behavior. We confirm the values of ${}_{fs}A_{60}(n_l)$ in Eq. (46) that can be immediately deduced from Tables I{IV}. The analytic results for ${}_{fs}A_{60}(n_l)$ are thus found to be consistent with the numerical data ${}_{fs}G_{SE}$; the level of confirmation is 5{10% [relative to ${}_{fs}A_{60}(n_l)$] for P and D states (1% for the 2P states, and

8D states not included for the reason mentioned above), 3 % for F states, and 1% for G states.

This represents an improvement over the accuracy of $A_{60}(n_l j)$ obtained by the previous check. This improvement comes evidently from the fact that the relative deviation of ${}_{\text{fs}}G_{\text{SE}}$ in Eq. (44) from ${}_{\text{fs}}A_{60}$ in Eq. (46) is small over the whole range $0 < Z \leq 110$, compared to the relative deviation

$$\frac{G_{\text{SE}}(n_l j; Z)}{A_{60}(n_l j)} \approx 1; \quad (48)$$

of G_{SE} [see Eq. (5)] from $A_{60}(n_l j)$ in Eq. (6) with $j = l+1=2$ or $j = l-1=2$. As a consequence, the uncertainty of the numerical evaluation of the limit of (47) as $Z \rightarrow 0$ is relatively small. Figure 10 shows an example of the smallness of the contributions to ${}_{\text{fs}}G_{\text{SE}}$ that go beyond ${}_{\text{fs}}A_{60}$. Moreover, we have observed that the higher the angular momentum l , the smaller the values of the deviation (47), hence the stronger confirmation of our values of ${}_{\text{fs}}A_{60}(n_l)$ for high orbital angular momenta. This point is also illustrated in Fig. 10.

V III. S U M M A R Y O F R E S U L T S

This paper contains results that are relevant to the self-energy of a non-S electron bound to a point nucleus of charge number Z . We provided estimates and values (see also Ref. [8]) for the first two non-analytically-known contributions to the self-energy expansion (5), namely the Bethe logarithm $\ln k_0(n_l)$ and the so-called $A_{60}(n_l j)$ coefficient, which can be viewed as a relativistic Bethe logarithm. The main numerical results are contained in Tables I{IV, in Eq. (35) and Table V III, in Eq. (36) and in Eq. (37). We have also conjectured, in Sec. V I, that the relativistic Bethe logarithm $A_{60}(n_l j)$ does not strongly depend on the principal quantum number n . In addition to this, we note that the orders of magnitude of $A_{60}(n_{l=1=2})$ and $A_{60}(n_{(l+1)_{l=3=2}})$ are the same, in Tables I{IV. All these results yield in particular, through Eqs. (1) and (7), the best available approximations of the self-energy in hydrogen and light hydrogenlike ions, except for $n = 1$ and $n = 2$ levels [11, 14] (see also Sec. V II); such an approximation can be obtained through Eqs. (1) and (7).

Calculating A_{60} has been a challenge since the seminal work of Bethe [4] on the dominant self-energy coefficients of S states [see Eqs. (7) and (1)]. Details of the method we used were described in Sec. III and IV. As discussed in Sec. V II, including the coefficients A_{60} reported in Tables I{IV in a (truncated) expansion of the self-energy improves its accuracy over a large range of nuclear charge numbers Z .

We checked our calculations of A_{60} by both analytic and numerical means. The so-called ϵ method, which we have employed (see Sec. III), makes divergences appear in the low- and high-energy contributions to A_{60} , as the scale-separating parameter ϵ between these two

contributions goes to zero. We have observed that, as required, these divergences cancel when the two parts are added. Moreover, our calculations correctly reproduced the known lower-order coefficients A_{40} and A_{61} . We have also checked our results for A_{60} against numerical values of the self-energy, and were able to confirm them by this independent method to the level of about 15 % (except for $D_{3=2}$ states, as explained in Sect. V II).

Obtaining results for A_{60} required extending (analytically) the angular algebra developed for 2P states [12] to higher angular momenta. Techniques of numerical convergence acceleration of series [6, 25, 27] were instrumental in evaluating the parts of A_{60} that could not be analytically calculated. The recent analytic calculations of Ref. [26] enabled us to obtain with a high precision the self-energy (1) of electrons with high ($j > 3=2$) angular momentum, for various values of the nuclear charge number Z ; the new calculations that we have performed required the use of massively parallel computers, and thousands of hours of computing time. (These numerical data, which have been used for the plots in Figs. 8{10, will be presented in detail elsewhere [57].) We have also collected the most recent available values of the self-energy. This provided us with independent values of the A_{60} coefficients, extracted from the numerical self-energies, thus allowing us to check the analytic results presented in Tables I{IV (see Sec. V II).

Severe cancellations appeared, between different contributions to A_{60} (in addition to the cancellation of the ϵ -parameter divergences): for some of the atomic states investigated, the absolute magnitude of the A_{60} coefficients is as small as 10^{-3} , whereas the largest individual contribution to A_{60} , when following the classification of the corrections according to Refs. [12, 13], is of the order of 10^2 or larger for all atomic states discussed here (see also Tables V I and V II).

Future calculations of the Bethe logarithm $\ln[k_0(n_l)=R_1]$ and of the relativistic Bethe logarithm $A_{60}(n_l j)$ could also fruitfully be compared to the estimates given by Eqs. (35), (36) and (37), and Table V III. The results presented in this paper also allow one to perform checks of future exact self-energies obtained by numerical methods, by comparing their values to the three-term self-energy approximation (42) provided here for P and higher- l states. The values of A_{60} in Tables I{IV can be of interest for analyzing the Lamb shift of highly-excited (high- n and high- l) electronic states in recent [7, 15, 16, 17] and future high-precision spectroscopy experiments. The results of Sect. IV {V I also provide the best available self-energy approximation for many states $n_l j$ and nuclear charge numbers Z (see Sec. V II); these approximations can for instance be useful in evaluating the contribution of QED effects in atoms [58, 59, 60, 61] or molecules [62].

Acknowledgments

The authors would like to acknowledge helpful discussions with K. Pachucki and J. Simons. We also thank the CINES (Montpellier, France) and the IDRIS (Orsay, France) for grants of time on parallel computers (IBM SP2 and SP3 [48]). E.O.L. acknowledges support from a Lavoisier fellowship of the French Ministry of Foreign Affairs, and support by NIST. U.D.J. acknowledges support from the Deutscher Akademischer Austauschdienst (DAAD). G.S. acknowledges support from BMBF, DFG and from GSI. The Kastler Brossel laboratory is Unité Mixte de Recherche 8552 of the CNRS.

APPENDIX : LOCAL FITS

This appendix describes a fitting procedure which is designed to extract "local" numerical quantities from a set of data points, and to allow one to assess the numerical uncertainty associated to these quantities. A partial sketch of this procedure was first introduced in Ref. [63]. Here, "local" refer for instance to the evaluation of a perturbation expansion about one abscissa; the purpose of the method presented here is to perform fits that are local to an abscissa of interest, as opposed to finding the best global fit of some data points. We thus used it in order to obtain asymptotic coefficients for $A_{60}(n_{\downarrow})$ for P and D states in Sec. V (see Table VIII), as well as the asymptotic expansion of the Bethe logarithm $\ln k_0(n_{\downarrow})$ in Eq. (37) in these applications, the quantities evaluated are local to either $n = 1$ or $l = 1$. This method can in principle be applied to many other problems that require local fits.

In order to describe the local-fit procedure, we take the evaluation of the limit

$$\lim_{l \rightarrow 1} l^3 \ln [k_0(n_{\downarrow}) = R_1] \quad (49)$$

as an example: here, we have $n = 1 + 1$, $\ln [k_0(n_{\downarrow}) = R_1]$ is the Bethe logarithm, and R_1 is the Rydberg constant. This limit was evaluated as $-0.056853(2)$ [see Fig. 2 and Eq. (37)].

Figures 2 and 11 contain data points which are relevant to (49): we have plotted

$$l^3 \ln [k_0(n_{\downarrow}) = R_1] \quad (50)$$

as a function of $l=1$ (with values of the Bethe logarithm found in Ref. [5]). The limit (49) can visually be estimated from the data points in Fig. 2 to be $-0.057(1)$.

In order to improve over the estimate $-0.057(1)$ for (49), we fit (exactly) each pair of two consecutive points (50) in Fig. 2 with a line [64], as depicted in Fig. 11. Each of the fitting lines in Fig. 11 gives an estimate of limit (49) by extrapolation to $l=1=0$ (intersection of the line with the $l=1=0$ axis). Figure 12 contains each of these estimates, as a function of the average abscissa of the two points that were used in obtaining

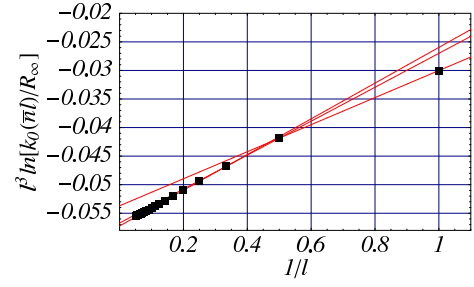


FIG. 11: This figure shows the lines going through a few pairs of successive data points (50) [see also Fig. 2]. Each of these lines is a local approximation to the curve underlying the data points. Each line yields an estimate of the limit (49) of the data points as $l=1 \rightarrow 0$ (this estimate is at the intersection of the line with the $l=1=0$ axis). Fig. 12 graphically displays these estimates.

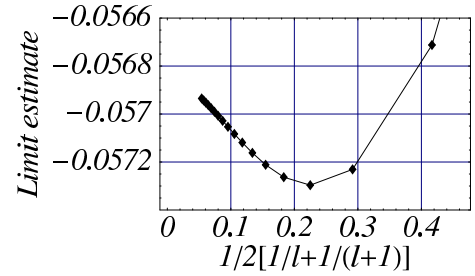


FIG. 12: This figure shows the estimates of limit (49) obtained through the two-point fits of Fig. 11. From this graph, we limit (49) to be $-0.0568(1)$, which is more precise than, and coherent with the value $-0.057(1)$ obtained from the original data points (50) in Figs. 2 and 11. The limit estimates are plotted along the vertical direction, while the abscissa associated to an estimate is the average abscissa of the two data points of Fig. 11 that were used in producing it.

it. Because the curve in Fig. 12 is relatively flatter than the curve in Fig. 11, we can estimate limit (49) with an improved uncertainty; thus, we deduce from Fig. 12 the value $-0.0568(1)$ for the limit (49) that we are studying, which is coherent with the previous estimate $-0.057(1)$.

This better estimate $-0.0568(1)$ of limit (49) can be improved by continuing to increase the number p of data points (50) included in local fits of the data. Thus, for an increasing number p of data points, we fitted (exactly) each set of p successive points (50) in Fig. 11 with a polynomial of degree $p-1$ (linear combination of the functions $1, l=1, \dots, l=1^{p-1}$), and represented the value of the polynomial extrapolated to $l=1=0$ as a function of the average abscissa of the p points. Fig. 13 depicts this process. The plotted values are estimates of the limit (49) obtained with higher and higher-order (local) fits of the data points (50). We observed that the curves so obtained become exponentially flat, in the sense that their relative amplitude become exponentially smaller and smaller until the uncertainties of individual estimates become important, as described below. This fact, which is illustrated in Fig. (13), allowed us to ob-

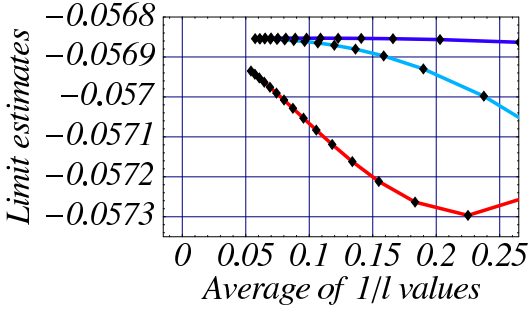


FIG. 13: From the lower to the higher curve: estimates of limit (49) obtained through fits of the data points (50) with polynomials of degree 1 (see also Fig. 12), 3 and 5 (see also Fig. 14). Fitting the data points (50) of Fig. (11) with 1 to 6 points yielded mutually coherent estimates of limit (49) with an exponentially decreasing error.

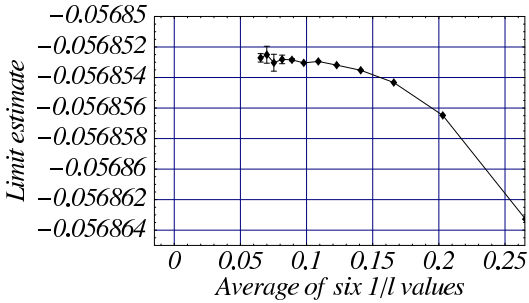


FIG. 14: This figure shows estimates of limit (49) obtained by fitting the data points (50) in Fig. 11 with fifth-degree polynomials (in $l=1$). The high relative stability of the estimates as $l=1 \rightarrow 0$ allowed us to give the precise value $0.056853(2)$ in Eq. (37) for limit (49).

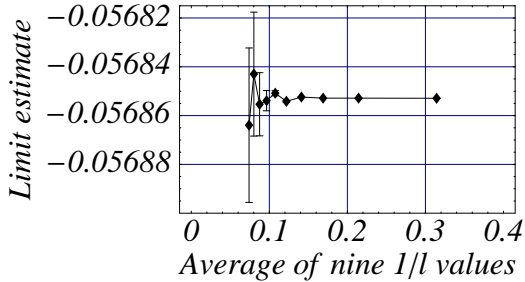


FIG. 15: This figure displays estimates of limit (49) obtained by fitting the data points (50) in Fig. 11 with a eighth-degree polynomials (in $l=1$). It should be compared to Fig. 14, which gives a more accurate estimate of limit (49) by fitting sequences of only six data points. The accuracy of the local fits performed here first increases with the order of the local approximations to the data points (50) (see Fig. 13), and then eventually decreases (compare this plot to Fig. 14).

tain more and more accurate estimates of limit (49).

The most accurate value that we obtained for limit (49) through the local-fit procedure described here

is $0.056853(2)$ [see Eq. (37)], as is illustrated in Fig. 14. This limit was obtained by fitting each sequence of $p = 6$ data points with a fifth-degree polynomial. Fits of the data points (50) with larger numbers of data points display more irregular estimate curves; this can for instance be seen by comparing Fig. 14 with Fig. 15.

As we have seen above, the uncertainty of the fitted value can be evaluated by visually prolongating the fitting curves (i.e., curves such as those of Figs. 12{15). Another uncertainty must in general be taken into account in order to obtain a reliable estimate for the fitted quantity: the uncertainty in the data points. All the curves presented in this appendix do contain error bars that reflect the uncertainties on the estimates of (49) that come from the uncertainties on the data points (50). We evaluated the uncertainty associated to each fit of p data points (50) by calculating three fits: a fit with the middle values of the ordinates, a fit with the higher values, and a fit with the lower values; the three estimates of the fitted quantity (49) obtained through this procedure define an estimate with an error bar (see, e.g., Fig. 15). Other ways of estimating the uncertainty in the fit result can be used; a good choice of uncertainty evaluation yields successive estimates of the fitted quantity that are compatible with a smooth curve of estimates [see, e.g., Fig. 15, where the less precise estimates of limit (49) lie in the prolongation of the more precise values, which are on the right of the plot].

One of the advantages of the local-fit method presented in this appendix is that data points that are located far from the abscissa of interest ($l=1 = 0$, here) can be fruitfully be used in evaluating the fitted quantity [limit (49), in our example]. Thus, as Fig. 15 illustrates, data points (50) with "large" abscissas can yield more precise estimates of limit (49) than data points with small abscissas. This behavior is particularly useful when data points in the region of interest have relatively large uncertainties.

The procedure detailed in this Appendix also allows one to study the quality of lists of numerical results that should lie on a smooth curve, but whose coherence is not obvious through a simple inspection or plot of the values. In fact, curves such as those found in Figs. 12{15 can be very sensitive to small errors in a list of numerical values. We have not noticed such errors in the A_{60} values Tables I and II while evaluating the asymptotic coefficients reported in Table V III; this provided an additional check of the values of these tables (see also Sec. V II).

The local-fit method described here is not restricted to the asymptotic study of the Bethe logarithm that we have used as an example. In general, it can yield precise estimates of quantities that are local to a set of data point [such as limit (49)], including, for instance, perturbation coefficients of non-analytic expansions [e.g., Eq. (5)].

- [1] F. Biraben, T. W. Hansch, M. Fischer, M. Niering, R. Holzwarth, J. Reichert, T. Udem, M. Weitz, B. de Beauvoir, C. Schwob, et al., in *The Hydrogen Atom: Precision Physics of Simple Atomic Systems*, edited by S. G. Karshenboim, F. S. Pavone, F. Bassani, M. Inguscio, and T. W. Hansch (Springer, 2001), *Lecture Notes in Physics*, p. 17.
- [2] P. J. Mohr and B. N. Taylor, *Rev. Mod. Phys.* **72**, 351 (2000).
- [3] G. W. Erickson and D. R. Yennie, *Ann. Phys. (N. Y.)* **35**, 271 (1965).
- [4] H. A. Bethe, *Phys. Rev.* **72**, 339 (1947).
- [5] G. W. F. Drake and R. A. Swainson, *Phys. Rev. A* **41**, 1243 (1990).
- [6] S. V. Aksenov, M. A. Savageau, U. D. Jentschura, J. Becher, G. So, and P. J. Mohr, *Comput. Phys. Commun.* **150**, 1 (2003).
- [7] J. C. DeVries, Ph.D. thesis, M.I.T. (2002).
- [8] U. D. Jentschura, E.-O. Le Bigot, P. J. Mohr, P. Indelicato, and G. So, *Phys. Rev. Lett.* (2003), [arXiv:physics/0304042](https://arxiv.org/abs/physics/0304042).
- [9] K. Pachucki, *Phys. Rev. A* **46**, 648 (1992).
- [10] K. Pachucki, *Ann. Phys. (N. Y.)* **226**, 1 (1993).
- [11] U. D. Jentschura, P. J. Mohr, and G. So, *Phys. Rev. Lett.* **82**, 53 (1999).
- [12] U. Jentschura and K. Pachucki, *Phys. Rev. A* **54**, 1853 (1996).
- [13] U. D. Jentschura, G. So, and P. J. Mohr, *Phys. Rev. A* **56**, 1739 (1997).
- [14] U. D. Jentschura, P. J. Mohr, and G. So, *Phys. Rev. A* **63**, 042512 (2001).
- [15] B. de Beauvoir, F. Nez, L. Julien, B. Cagnac, F. Biraben, D. Touahri, L. Hilico, O. Acaf, A. Clairon, and J. J. Zondy, *Phys. Rev. Lett.* **78**, 440 (1997).
- [16] C. Schwob, L. Jozefowski, B. de Beauvoir, L. Hilico, F. Nez, L. Julien, F. Biraben, O. Acaf, and A. Clairon, *Phys. Rev. Lett.* **82**, 4960 (1999).
- [17] C. Schwob, L. Jozefowski, B. de Beauvoir, L. Hilico, F. Nez, L. Julien, F. Biraben, O. Acaf, J.-J. Zondy, and A. Clairon, *Phys. Rev. Lett.* **86**, 4193 (2001).
- [18] J. Reichert, M. Niering, R. Holzwarth, M. Weitz, T. Udem, and T. W. Hansch, *Phys. Rev. Lett.* **84**, 3232 (2000).
- [19] M. Niering, R. Holzwarth, J. Reichert, P. Pokasov, T. Udem, M. Weitz, T. W. Hansch, P. Lemonde, G. Santarelli, M. Abgrall, et al., *Phys. Rev. Lett.* **84**, 5496 (2000).
- [20] B. de Beauvoir, C. Schwob, O. Acaf, L. Jozefowski, L. Hilico, F. Nez, L. Julien, A. Clairon, and F. Biraben, *Eur. Phys. J. D* **12**, 61 (2000).
- [21] P. J. Mohr, G. Plunien, and G. So, *Phys. Rep.* **293**, 227 (1998).
- [22] P. Indelicato and P. J. Mohr, *Phys. Rev. A* **58**, 165 (1998).
- [23] P. J. Mohr, *Ann. Phys. (NY)* **88**, 26 (1974).
- [24] P. J. Mohr, *Ann. Phys. (NY)* **88**, 52 (1974).
- [25] U. D. Jentschura, Ph. D. thesis, Dresden University of Technology, published as "Quantum Electrodynamical Radiative Corrections in Bound Systems," *Dresdner Forschungen: Theoretische Physik, Band 2* (w.e.b. Universitätsverlag, Dresden, 1999).
- [26] E.-O. Le Bigot, P. Indelicato, and P. J. Mohr, *Phys. Rev. A* **64**, 052508 (2001).
- [27] U. D. Jentschura, P. J. Mohr, G. So, and E. J. Weniger, *Comput. Phys. Commun.* **116**, 28 (1999).
- [28] G. W. Erickson and D. R. Yennie, *Ann. Phys. (N. Y.)* **35**, 447 (1965).
- [29] G. W. Erickson, *Phys. Rev. Lett.* **27**, 780 (1971).
- [30] J. Sapirstein, *Phys. Rev. Lett.* **47**, 1723 (1981).
- [31] S. G. Karshenboim, *Z. Phys. D* **39**, 109 (1997).
- [32] J. Sapirstein and D. R. Yennie, *Quantum Electrodynamics* (World Scientific, Singapore, 1990), pp. 560-672.
- [33] S. Karsfeld and A. Maquet, *Phys. Lett. B* **43**, 201 (1973).
- [34] H. A. Bethe, L. M. Brown, and J. R. Stehn, *Phys. Rev.* **77**, 370 (1950).
- [35] J. M. Harriman, *Phys. Rev.* **101**, 594 (1956).
- [36] C. Schwartz and J. J. Thiemann, *Ann. Phys. (N. Y.)* **6**, 178 (1959).
- [37] M. Lieber, *Phys. Rev.* **174**, 2037 (1968).
- [38] R. W. Hu, *Phys. Rev.* **186**, 1367 (1969).
- [39] R. C. Forrey and R. N. Hill, *Ann. Phys. (N. Y.)* **226**, 88 (1993).
- [40] S. E. Haywood and J. D. Morgan III, *Phys. Rev. A* **32**, 3179 (1985).
- [41] M. Abramowitz and I. A. Stegun, eds., *Handbook of mathematical functions* (Dover publications, Inc., New York, 1972), 9th ed.
- [42] K. Pachucki, *Phys. Rev. A* **48**, 2609 (1993).
- [43] U. D. Jentschura and K. Pachucki, *J. Phys. A* **35**, 1927 (2002).
- [44] E. H. Wichmann and C. H. Woo, *J. Math. Phys.* **2**, 178 (1961).
- [45] L. Hostler, *J. Math. Phys.* **11**, 2966 (1970).
- [46] A. R. Edmonds, *Angular Momentum in Quantum Mechanics* (Princeton University Press, Princeton, NJ, 1957).
- [47] S. Wolfram, *Mathematica—A System for Doing Mathematics by Computer* (Addison-Wesley, Reading, MA, 1988).
- [48] Certain commercial equipment, instruments, or materials are identified in this paper to foster understanding. Such identification does not imply recommendation or endorsement by the National Institute of Standards and Technology, nor does it imply that the materials or equipment identified are necessarily the best available for the purpose.
- [49] F. W. J. Olver, *Asymptotics and Special Functions* (Academic Press, New York, NY, 1974).
- [50] H. Bateman, *Higher Transcendental Functions*, vol. 1 (McGraw-Hill, New York, NY, 1953).
- [51] E. J. Weniger, *Comput. Phys. Rep.* **10**, 189 (1989).
- [52] G. W. Erickson, *Journal of Chemical Reference Data* **6**, 831 (1977).
- [53] S. Kotochigova, P. J. Mohr, and B. N. Taylor, *Can. J. Phys.* **80**, 1373 (2002).
- [54] P. J. Mohr and Y.-K. Kim, *Phys. Rev. A* **45**, 2727 (1992).
- [55] P. J. Mohr, *Phys. Rev. A* **46**, 4421 (1992).
- [56] P. Indelicato and P. J. Mohr, *Hyperne Interact.* **114**, 147 (1998).
- [57] E.-O. Le Bigot, U. D. Jentschura, P. J. Mohr, and P. Indelicato, to be submitted.
- [58] U. Feldman, J. Sugar, and P. Indelicato, *J. Opt. Soc.*

- Am. B 8, 3 (1990).
- [59] F. Parente, J. P. Marques, and P. Indelicato, Eur. Phys. Lett. 26, 437 (1994).
- [60] D. R. Beck, Phys. Rev. A 56, 2428 (1992).
- [61] J. Sugar, V. Kaufman, P. Indelicato, and W. L. Rowan, J. Opt. Soc. Am. B 6, 1437 (1989).
- [62] P. Pyykko, K. G. Dyall, A. G. Csaszar, G. Tarczay, O. L. Polyansky, and J. Tennyson, Phys. Rev. A 63, 024502 (2001).
- [63] P. J. Mohr, Phys. Rev. Lett. 34, 1050 (1975).
- [64] In general, each such pair of points should be (exactly) fitted with a linear combination of the first two functions of the perturbation expansion of the data points about the abscissa of interest. For instance, an evaluation of $A_{40}(n_l_j) = \lim_{Z \rightarrow 0} F(n_l_j; Z)$ in Eq. (7) would require fitting each pair of data points $(Z_j; F(n_l_j; Z_j))$ with a linear combination of the functions 1 (constant) and $(Z_j)^2 \ln[(Z_j)^2]$.